Magnetic Nanoparticles

A. Feoktystov

This document is a slightly revised version of an article originally published in

Manuel Angst, Thomas Brückel, Dieter Richter, Reiner Zorn (Eds.):
Scattering Methods for Condensed Matter Research: Towards Novel Applications at Future Sources
Lecture Notes of the 43rd IFF Spring School 2012
Schriften des Forschungszentrums Jülich / Reihe Schlüsseltechnologien / Key Technologies, Vol. 33
JCNS, PGI, ICS, IAS
Forschungszentrum Jülich GmbH, JCNS, PGI, ICS, IAS, 2012
ISBN: 978-3-89336-759-7

E 6 Magnetic Nanoparticles

A. Feoktystov
Jülich Centre for Neutron Science
Forschungszentrum Jülich GmbH

Contents

Lecture Notes of the 43rd IFF Spring School "Scattering Methods for Condensed Matter Research: Towards Novel Applications at Future Sources" (Forschungszentrum Jülich, 2012).

1 Introduction

Nowadays materials with nanosized particles are of great interest due to their completely different properties as compared to the bulk. The knowledge about the behaviour of such nanomaterials is of great importance. This will give the base for the future development of substances with the given or controlled properties.

In this lecture we will learn quite new and promising substance – magnetic fluid. As a research method, the small-angle neutron scattering (SANS) will be presented. A powerful technique of contrast variation will be discussed in details and applied to small-angle neutron scattering on magnetic fluids. We will see that small-angle neutron scattering investigations of magnetic fluids give important information about particle structure and their interaction.

2 Magnetic Fluids and their Applications

Magnetic fluids (or ferrofluids) are colloidal dispersions of magnetic nanoparticles in liquids. The typical particle size is around 10 nm. The size of the particles is below the critical size, so that such small particles become single domain in contrast to bulk ferromagnetic material which has domain structure of magnetization. The single domain nanoparticles have saturation magnetization. To prevent aggregation of the particles because of the dipole-dipole interaction (especially under influence of the external magnetic field) particles are usually coated with a stabilizing surfactant layer [1]. While in the case of non-polar organic carriers one surfactant layer chemisorbed on the surface of magnetic particles is enough for this purpose (Fig. 1*a*), for polar magnetic fluids the double stabilization, conventionally the formation of the additional second layer, is required [2,3]. In this case, the first layer forms due to chemisorption of surfactant polar heads on the surface of the magnetic particles. The second layer is the result of the physical sorption: tails of the second layer's molecules are turned to the tails of the first layer's molecules, thus polar heads of molecules of the second layer are turned outside, which makes it possible to dissolve the particles in polar carriers.

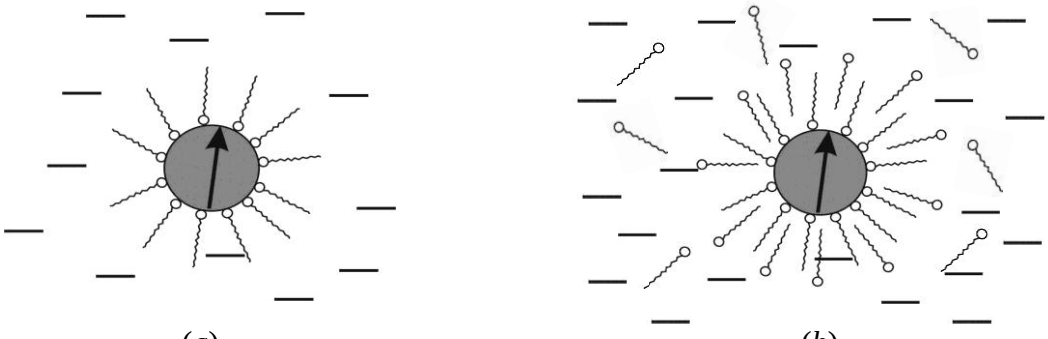

(*a*) (*b*)

Fig. 1: *Schematic representation of nanoparticles in non-polar (a) and polar (b) magnetic fluid. Note excess of surfactant in solution in case of polar ferrofluids.*

Such kind of double-layer stabilization requires some excess of the surfactant molecules in the solution, so that exchange of molecules of the second stabilization layer with free molecules in the solvent is in equilibrium (Fig. 1*b*).
Due to the combination of magnetic properties and liquidity ferrofluids found a large variety of applications. All the applications are based on the principles that under the influence of magnetic field the ferrofluid goes to the point where the magnetic field is the strongest, absorption of electromagnetic energy at convenient frequencies causes the ferrofluid heat up and the ferrofluid properties can be changed with the application of magnetic field.

2.1 Technical applications

Technical applications consider the ferrofluids' properties as a whole. In techniques magnetic fluids are already used in dynamic sealing, damping, bearings, separation, heat dissipation, measuring devices and so on [4,5]. We will stop here in more details on the applications of magnetic fluids for heat dissipation and dynamic sealing.
Ferrofluids are used to form liquid seals around the spinning drive shafts in hard disks, which have to operate in a hermetically closed box because any grain of powder or even smoke may spoil the reading and writing process. This is achieved by making the hole inside a magnet and the shaft made of soft magnetic material. A groove in the shaft is filled up with ferrofluid, which is kept in place by the magnetic field, obstructing the passage of any impurity, but leaving the axle free to rotate, because the obstructing material is liquid [4,5].
Another good example of ferrofluid application is loudspeaker. Its coil heats up by functioning and the ferrofluid is kept in place by the magnetic field of the magnet which is fixed on the loudspeaker's horn. When the magnetic fluid temperature reaches Curie temperature, ferrofluid's particles lose their magnetic properties and a non-magnetic liquid would flow away and will be substituted by a part of the fluid which has not been overheated. In this case a passive heat transfer is realized. Nowadays most of the high power loudspeakers are equipped with ferrofluid. The presence of the fluid around the coil improves also the quality of the speaker because it damps unwanted resonances, which would produce a very unpleasant noise [5].

2.2 Biomedical applications

In contrast to technical applications biomedical applications of magnetic fluids focus on the single colloids' properties. The main direction of ferrofluids' application in biomedicine is cancer treatment. It is magnetic hyperthermia [4,5,6], drug targeting and delivery [5,7], contrast medium in Magnetic Resonance Imaging (MRI) [5,6,7].
When one applies a drug onto the surface of magnetic particle and focuses the nanoparticles around cancer tumor with the external magnetic field, the amount of drug necessary is much less than what would be necessary if it were dispersed in the whole body. When the magnetic field is turned off the drug will disperse in the body, but, since the total amount is very small, there will be practically no side effects [5].
The powerful technique of MRI is based on the different relaxation times T_2 of the proton's magnetic moments when it is inside different environments. Often the differences are not strong enough to obtain well resolved images. Dextran coated iron oxides are biocompatible and are excreted via the liver after the treatment. They are selectively taken up by the

reticuloendothelial system. This is important because tumor cells do not have the effective reticuloendothelial system of healthy cells, so that their relaxation time is not altered by the contrast agent, which makes them distinguishable from the surrounding healthy cells [5,8].
Hyperthermia is a promising therapy technique which is based on the property of ferrofluids to absorb electromagnetic energy at a certain frequency. This allows one to heat up a localized portion of a living body, where ferrofluid has been injected, for example a tumor, without heating at the same time the surrounding parts of the body. The results of successful experiments healing cancer tumors in rats and rabbits can be found in [9].
The main problem of Hyperthermia is the high Curie temperature of the used ferromagnetic materials. The solution is to define substances with low Curie temperature in order to avoid possible harmful overheating of the human body [10].

3 Magnetic Properties of the Nanoparticles

In bulk ferromagnets the magnetization has a domain structure. These domains form to minimize the magnetostatic energy of the material. As the size of a magnetic particle is reduced down to the critical one the magnetic properties of the material are then dictated by the particle anisotropy and shape rather than by the microstructure of the bulk magnets. There are two main sources of magnetic anisotropy – magnetocrystalline anisotropy and shape anisotropy. Magnetocrytalline anisotropy is determined by the atomic structure of a crystal, which introduces preferential directions for the magnetization (easy axes). The easy and hard directions arise from the interaction of the spin magnetic moment with the crystal lattice (spin-orbit coupling). Shape anisotropy appears when a particle is not perfectly spherical. The demagnetizing field will not be equal for all directions, creating one or more easy axes.

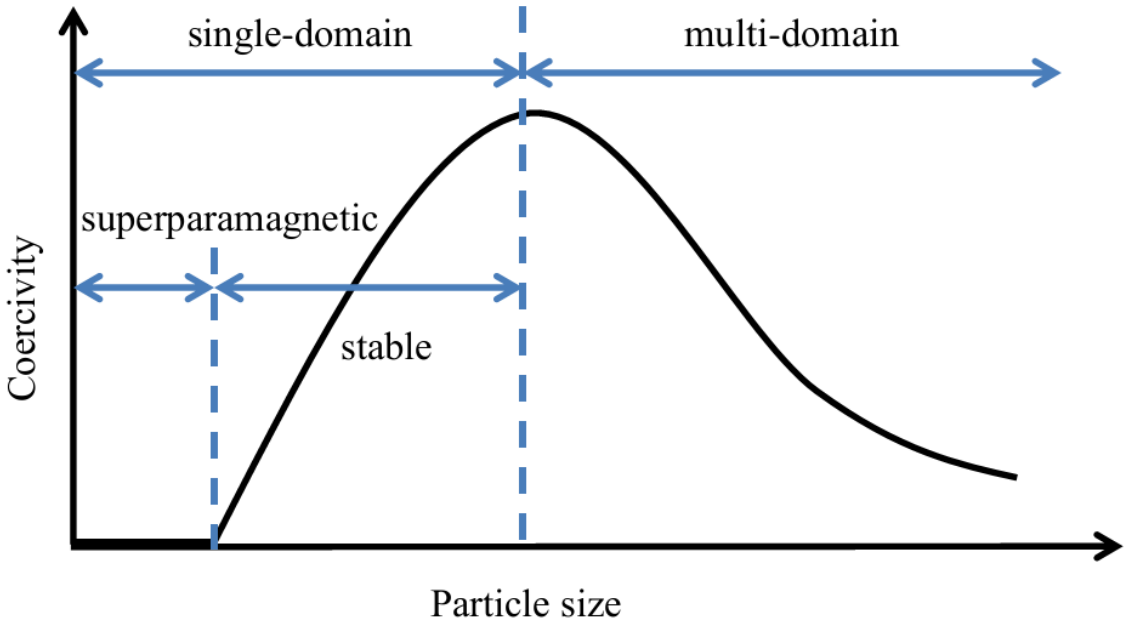

Fig. 2: *Coercivity as a function of particle size.*

Let's have a look on coercivity as a function of particle size (Fig. 2). For large sizes the particles are multi-domain becoming more bulk-like with increasing size. Below a critical particle size domain walls will no longer form due to energy considerations and single domain particles are stable. This critical size corresponds to the peak in the coercivity in Fig. 2. The peak position on the particle size axis is dependent on the values of anisotropy and magnetization. Below the coercivity maximum the particles remain stable until the effects of temperature destroy the ferromagnetic order. The particles are then superparamagnetic. The superparamagnetic size strictly depends on the magnetocrystalline anisotropy of the material [11].

3.1 Superparamagnetism

An assembly of non-interacting single-domain isotropic particles behaves like classical paramagnetic matter but with very high ($\sim 10^3 - 10^4\ \mu_B$) effective magnetic moment μ per particle [12]. If the influence of thermal energy is high enough the magnetic moments of the nanoparticle are randomized unless a magnetic field is applied. In thermal equilibrium the average magnetic moment of assemble has the following expression [12]:

$$< \mu >= \mu \cdot (\coth(\mu H / kT) - kT / \mu H) . \qquad (1)$$

Such substances with a huge magnetic susceptibility, whose average magnetic moment is represented by equation (1), are called then superparamagnetic.

3.2 Néel relaxation. Blocking temperature

Equation (1) is valid only in case of negligible anisotropy energy, but real single-domain particles are anisotropic. In the normal conditions the magnetization direction inside particle is along the easy axis. The two states of magnetization of a uniaxial magnetic particle are separated by an energy barrier (Fig. 3), K_uV, where K, is the anisotropy energy density and V is the particle volume [11]. If the thermal energy, kT, becomes comparable to the barrier height there is an increased probability of the magnetization reversing.

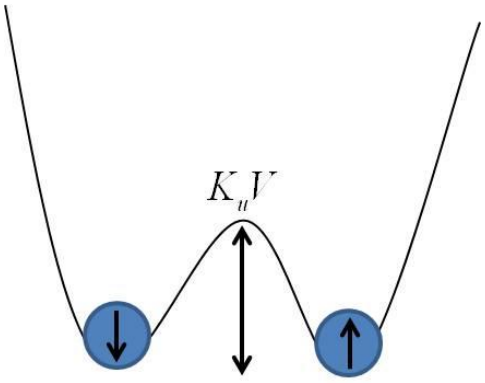

Fig. 3: *Double potential well with two possible orientations of particle magnetic moment.*

This thermally activated switching in case of non-interacting single-domain nanoparticles with the uniaxial magnetic symmetry follow the Née1 relaxation law [12]:

$$\tau = \tau_0 \exp(\frac{K_u V}{kT}), \quad (2)$$

where τ is the relaxation time and τ_0 is a constant.
In case of hard disks stability over a time scale of, for example, 10 years gives a stability criterion of $K_u V/kT > 40$ [13].
The value of τ_0 is typically in the range 10^{-13} –10^{-9} s [12,14]. The actual magnetic behavior of nanoparticle assemble depends on the value of the measuring time, τ_{exp}, of the specific experimental technique with respect to the relaxation time.
If $\tau_{exp} >> \tau$, the relaxation is fast and a time average of the magnetization orientation is observed during the measurement time. In this case the assembly of nanoparticles behaves like a paramagnetic system. If $\tau_{exp} << \tau$, the relaxation is slow and non-equilibrium properties are observed. The two cases are separated by the blocking temperature, T_B. It can be defined from the expression $\tau_{exp} = \tau$:

$$T_B = \frac{K_u V}{k} \ln^{-1}\left(\frac{\tau_{exp}}{\tau_0}\right). \quad (3)$$

Near T_B changes of magnetization reorientation occur with relaxation times comparable with the time of a measurement. Well below T_B the thermal agitation can be neglected and magnetization has static behavior.
It is quite hard to define T_B uniquely. The values of τ_{exp} depend on the experimental technique. In case of Mossbauer spectroscopy τ_{exp} is of the order of a few nanoseconds while in static magnetization measurements the timescale is typically of the order of 1 s. Therefore, the same nanoparticles can be in the superparamagnetic state in static magnetization experiments and in the blocked state in Mossbauer spectroscopy experiments [12,14].
Nevertheless, there are some general properties of the T_B: the blocking temperature increases with nanoparticle size increase and for a given particle size increases with decreasing measuring time. The highest possible value of T_B is represented by the Curie (or Néel) temperature, when the magnetic moments of each particle disappear [12].

4 Small-Angle Neutron Scattering

There are several possible ways for neutron to interact with a matter. In general, neutrons can be absorbed or captured with all the corresponding consequences or neutrons can scatter on the atoms and inhomogeneities either elastically or inelastically. Small-angle neutron scattering (SANS) is an elastic coherent scattering of neutrons [15]. The typical neutron wavelength used in SANS experiments is in the order of several angstroms [16]. Since distances between atoms in a substance are of the same order as neutron wavelength the coherent scattering picture is concentrated in small-angle region. That is why this method

received its name. In SANS experiment one registers a dependence of scattering cross-section (scattering intensity *I*) on modulus of scattering vector *q* (i.e. on scattering angle):

$$q = \frac{4\pi}{\lambda}\sin\theta, \tag{4}$$

where λ is the neutron wavelength and 2θ is the scattering angle.
The intensity of small-angle neutron scattering is a superposition of particle form- and structure factors. From the form-factor dependence on the scattering angle one obtains information about distribution of the scattering density inside scattering particles (size, shape, etc.). The structure-factor gives information about particle displacement (radial distribution function).
In 1939 Guinier derived a general expression for the *q*-dependence of scattering intensity at small angles, which gives number of scattering parameters directly from scattering curve [15]:

$$I(q \sim 0) = I(0)\exp\left(-\frac{R_g^2 q^2}{3}\right). \tag{5}$$

Here *I*(0) is called zero scattering intensity and contains information about amount of the scattering particles and R_g is a gyration radius, which as in mechanics is directly connected to particle dimensions.

4.1 Contrast variation. Basic functions

In contrast to X-ray scattering the amplitude of neutron scattering depends on atomic number in random way. Thus, for example, it made it possible to detect signal from hydrogen containing substances of the background of heavy atoms such as iron, copper and so on.
If we consider particles placed in the certain solvent, we have to take into account that the scattering intensity will not be proportional just to square of the average particle scattering density but to the square of difference between the average scattering density of the particles and scattering density of the solvent. This difference is called contrast. If the scattering densities of the particle and of the solvent are equal the neutrons doesn't "see" the particles, since the solution represents a homogeneous continuum, and waves scattered into any direction will be extinguished. The neutrons give a brilliant possibility to study complex structures "step-by-step" since one can use hydrogen/deuterium substitution in the solvent or in some part of the particle. It will significantly change scattering contrast of the system revealing scattering features that were buried in case of fully protonated system. The idea and theory of such influence on system contrast was developed by H.B. Stuhrmann and is known as contrast variation [17].
He showed that scattering intensity can be expanded into series of contrast [17]:

$$I(q) = I_s(q) + \Delta\rho I_{cs}(q) + (\Delta\rho)^2 I_c(q), \tag{6}$$

where I_s, I_{cs} and I_c are called basic functions, $\Delta\rho$ is a contrast. I_s gives the residual scattering at zero contrast – scattering on density fluctuations. I_c dominates at high contrasts and represents thus the scattering intensity of the particle shape. I_{cs} is a cross-term.
The parameters of Guinier approximation (5) have the following dependences (see for example [18]):

$$I(0) = nV_c^2(\Delta\rho)^2 \text{ and } R_g^2 = R_c^2 + \alpha/\Delta\rho - \beta/(\Delta\rho), \tag{7}$$

where R_c and V_c are particle gyration radius and corresponding volume, n particle number density, α and β are the parameters describing the relative distribution of the "heavy" and "light" components inside particles [16].
This is only valid for monodisperse non-magnetic particles. In case of polydisperse and magnetic particles, whose scattering density also depends on size, one has to make averaging of equation (6) over the particle size distribution function. Nevertheless, as it was shown in [18] it is still possible to derive the final expression to the same form as (6), but with modified basic functions and modified contrast:

$$I(q) = \tilde{I}_s(q) + \Delta\tilde{\rho}\tilde{I}_{cs}(q) + (\Delta\tilde{\rho})^2\tilde{I}_c(q). \tag{8}$$

Here $\Delta\tilde{\rho}$ is the modified contrast – the difference between effective average scattering density of the particles $\bar{\rho}_e$ and solvent [18].
Since magnetic scattering doesn't depend on contrast, its contribution enters into the $\tilde{I}_s$ modified basic function. Among all of the modified basic functions, which are now the expressions of classical basic functions, the modified basic function $\tilde{I}_c$ is just the average of the classical shape scattering basic function I_c over the polydispersity function.
The parameters of Guinier approximation have qualitatively different from (see [18] for more details):

$$I(0) = n(\Delta\tilde{\rho})^2 < V_c^2 > + n < (\bar{\rho} - \bar{\rho}_e)^2 V_c^2 > + (2/3)n\rho_m^2 < V_m^2 >, \tag{9a}$$

$$\tilde{R}_g^2 = \left[\frac{< V_c^2 R_c^2 >}{< V_c^2 >} + \frac{A}{\Delta\tilde{\rho}} - \frac{B}{(\Delta\tilde{\rho})^2} \right] \Big/ \left[1 + \frac{D}{(\Delta\tilde{\rho})^2} \right], \tag{9b}$$

where ρ_m and V_m are magnetic scattering density and magnetic volume of the particle, A, B, D are parameters and <…> denote averaging over polydispersity function. Now it is impossible to find a scattering density of the solvent which would zero contrast from all of the particles in solution simultaneously, so there is always residual scattering intensity at the effective match point (where $\Delta\tilde{\rho} = 0$): due to polydispersity (the second summand in equation (9*a*)) and contrast independent magnetic scattering (the third summand in equation (9*a*)).

4.2 Core-shell structure

Magnetic nanoparticles in ferrofluids are of core-shell structure. As an example let's consider a simple case of monodisperse non-magnetic nanoparticles (Fig. 4).

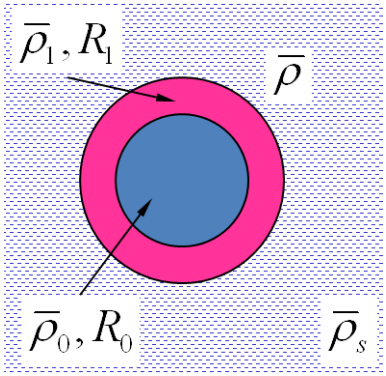

Fig. 4: *Schematic representation of the particle core-shell structure.* $\overline{\rho}_0$ *and* $\overline{\rho}_1$ *are scattering densities of the particle core and shell (* $\overline{\rho} = (V_0/V_1)\rho_0 + (1-V_0/V_1)\rho_1$ *is the average particle scattering density),* $\overline{\rho}_s$ *is solvent scattering density.* R_0 *and* R_1 *are the radii of particle core and shell.*

The expression for scattering intensity in this case consists of the core and shell contributions:

$$I(q) = n[(\overline{\rho}_1 - \overline{\rho}_s)V_1\Phi(qR_1) - (\overline{\rho}_1 - \overline{\rho}_0)V_0\Phi(qR_0)]^2, \tag{10}$$

where V_0 and V_1 are the particle and "particle+shell" volumes and $\Phi(x)$ is the spherical scattering amplitude: $\Phi(x) = 3(\sin x - x\cos x)/x^3$ [16].
Combining the members at contrast $\Delta\rho = \overline{\rho} - \overline{\rho}_s$, the three basic functions in equation (6) can be derived analytically:

$$I_s(q) = nV_0^2(\overline{\rho}_1 - \overline{\rho}_0)^2[\Phi(qR_1) - \Phi(qR_0)]^2, \tag{11a}$$

$$I_{cs}(q) = 2nV_1V_0(\overline{\rho}_1 - \overline{\rho}_0)\Phi(qR_1)[\Phi(qR_1) - \Phi(qR_0)](\Delta\rho), \tag{11b}$$

$$I_c(q) = nV_1^2\Phi^2(qR_1)(\Delta\rho)^2. \tag{11c}$$

To obtain the three basic functions one has to measure scattering curves for at least three contrasts, then the system of equations of type (6) can be easily solved and compared to the analytical result.
In case of magnetic nanoparticles one has to add a magnetic contribution in equation (10), the square of magnetic form-factor F_M:

$$F_M^2(q) = [\rho_m V_m \Phi(qR_m)]^2. \tag{12}$$

In case of SANS with non-polarized neutrons on diluted unmagnetized samples of ferrofluids, the total scattering intensity contains contributions of nuclear form-factor and 2/3 of magnetic form-factor (for more details refer to [19]):

$$I(q) = F_N^2(q) + \frac{2}{3} F_M^2(q) . \tag{13}$$

As a first example we consider organic magnetic fluids which are polydisperse magnetite (Fe_2O_3) nanoparticles coated with a single layer of oleic (OA) or myristic acid (MA) in benzene [20].

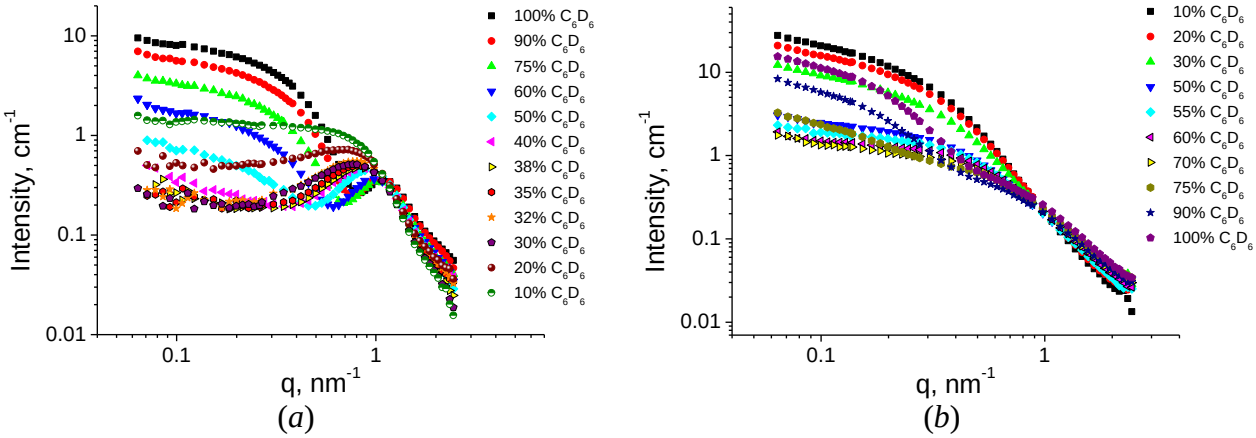

Fig. 5: *Contrast variation curves of SANS on diluted ferrofluids: (a) – MA stabilization, (b) – OA stabilization. The amount of D-benzene in the solvent (i.e. contrast) is indicated in the legend.*

For changing system contrast initial concentrated magnetic fluids (based on C_6D_6) were diluted with different mixtures of D- and H-benzene, so that the D-benzene content in the final solution was varied within interval 10-100 % (10–12 points). The final magnetic particle concentrations in ferrofluids were 0.8 % and 0.7 % in case of MA and OA stabilization respectively. The whole set of obtained scattering curves at different contrast are presented in Fig. 5.

To each of the scattering curves in Fig. 5 the Guinier approximation (5) was applied and the dependences (9) were obtained (Fig. 6):

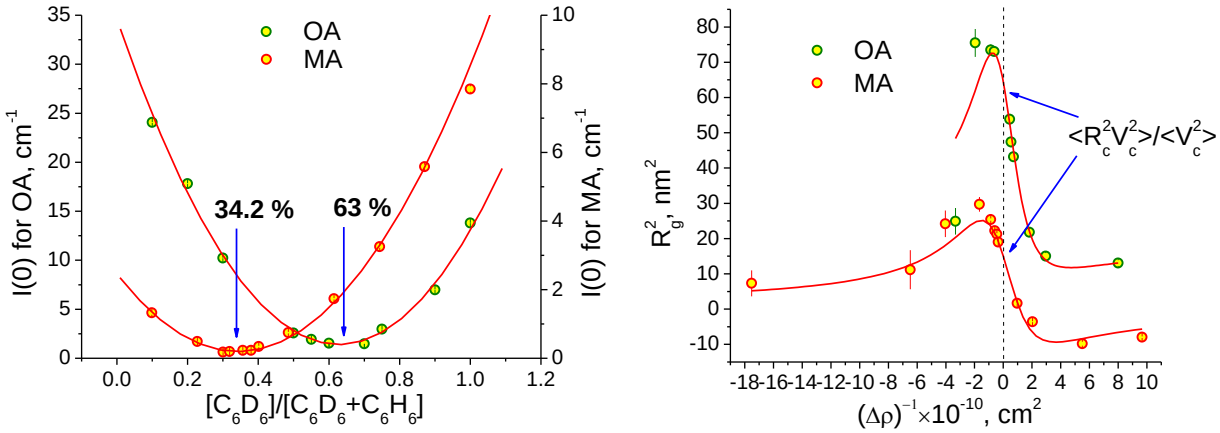

Fig. 6: *The parameters of the Guinier approximation (5) fitted according to equations (9). (a) – zero scattering intensity dependence on deuteration of the solvent and (b) – dependence of gyration radius on inversed contrast.*

The effective match points were determined from parabolic fitting of curves in Fig. 6*a* as 34.2 ± 0.4 % and 63 ± 3 % of the D-benzene content for MA and OA fluids, respectively. The corresponding scattering density's values are (2.64 ± 0.03) × 10^{10} cm^{-2} and (3.86 ± 0.15) × 10^{10} cm^{-2}. Taking into account the quasi-spherical shape of particles in magnetic fluids the characteristic radius of the whole particle was calculated from the fit results were calculated to be 5.0 ± 0.1 nm (MA) and 10.3 ± 0.1 nm (OA) [20]. Thus, combining the results of the calculated effective match point, which shows that OA sample contains more of heavier component (magnetite) in the particles, and radius of the particles one can speak about size regulation effect when using such two surfactants to synthesize the ferrofluids. The particle size, which comprises both the mean size and polydispersity, in OA fluid is twice larger as compared to MA fluid.

From the whole set of scattering curves the three basic functions from equation (8) were calculated. The best way to check the reliability of the calculated basic functions is to compare I_s basic function, which is a residual scattering intensity at zero contrast, with the scattering curve close to math point (Fig. 7). As one can see, the I_s basic functions coincide well with measured SANS curves which confirms correctness if the basic function separation. Comparison of the shape scattering basic functions I_c for two magnetic fluids directly confirms the results of fit of gyration radius dependence on inversed contrast in Fig. 6*b* with the expression (9*b*). The I_c basic function in case of OA stabilization is more steep than MA sample, which is the results of larger particles in the ferrofluid.

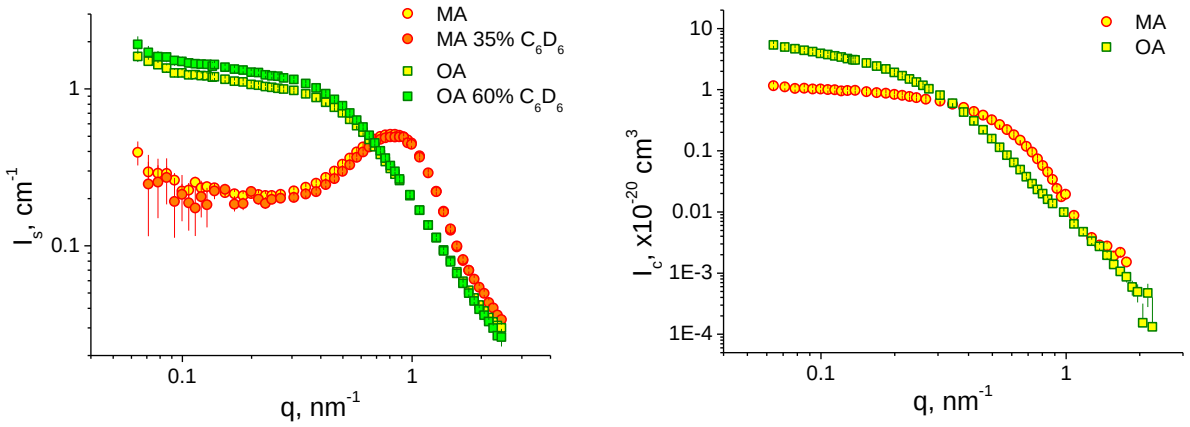

(*a*) (*b*)

Fig. 7: *Calculated basic functions of expression (8). (a) represents I_s basic function of the residual scattering and (b) – I_c shape scattering basic functions. I_{cs} is not shown due to the lack of its transparent interpretation.*

For the next example we consider water-based magnetic fluids. Performing the same steps for sample dilution with different ratios of H_2O and D_2O as for previous ferrofluids the SANS contrast variation curves were measured in 10 contrast points for each sample (Fig. 8) [21,22].

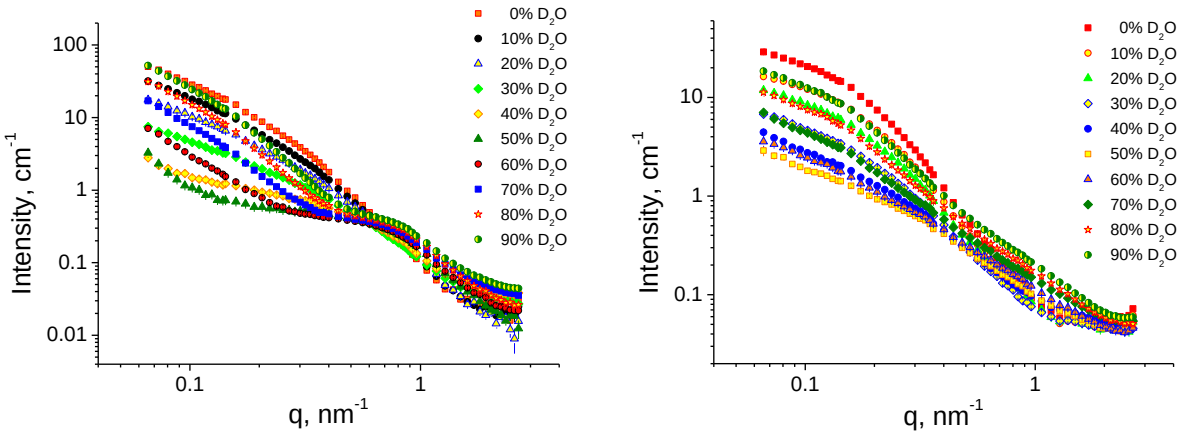

(*a*) (*b*)

Fig. 8: *SANS contrast variation curves for water-based magnetic fluids with double layers of lauric (LA) (a) and myristic acid (MA) stabilization (b). The ration of D_2O in the solvent is indicated in the legend.*

As one can see, Guinier region, which is represented by a plateau at small *q*-values, is inaccessible here due to an aggregation in ferrofluids. The water-based magnetic fluids require double stabilizing shell around magnetic nanoparticles. The second layer is quite weak and its molecules are in equilibrium with the free surfactant in the solvent. The equilibrium is very sensitive to external actions and such ferrofluids are usually characterized by the existence of aggregates (see for example [23]).

Nevertheless, the three basic functions (8) were calculated, among them the most informative shape scattering basic function I_c (Fig. 9*a*). From the more steep I_c curve of LA magnetic fluid one can easily say that particles (aggregates) in the sample are large than in MA sample.

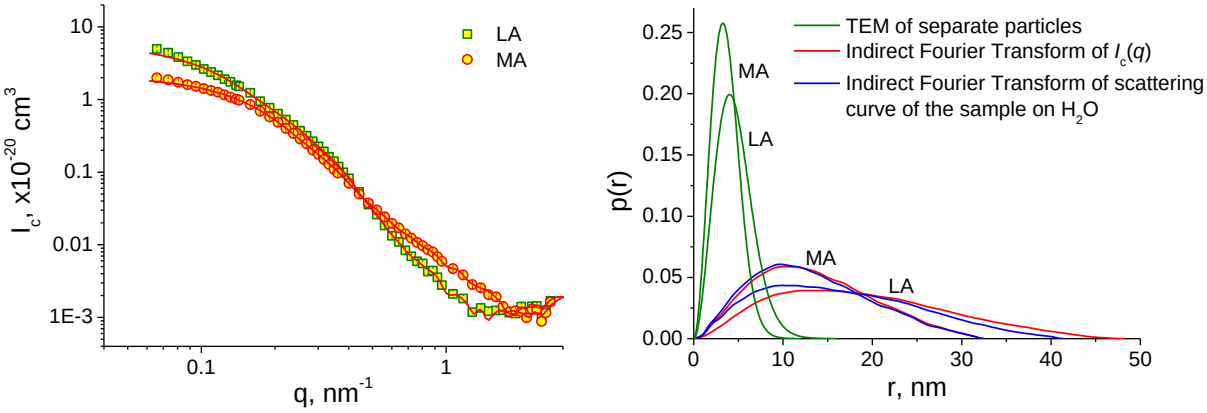

(*a*) (*b*)

Fig. 9: *Shape scattering basic functions for both ferrofluids. Line shows fit according to Indirect Fourier Transformation [24] (a). The pair distance distribution functions calculated from the shape scattering basic functions, scattering curves of the samples in pure H_2O and compared to the results of Transmission Electron Microscopy measurements [22] (b).*

The comparison of pair distribution functions calculated from I_c basic function and scattering curves of ferrofluids on H_2O, where due to a weak contrast between shell and water the scattering originates mainly from magnetite core, are compared to the results of Transmission Electron Microscopy, when only single particles were taken into account (Fig. 9*b*). In both cases experimental curves give broader $p(r)$ function pointing to the existence of large aggregates in the samples. In case of LA sample the maximum r-value of $p(r)$ functions are different on 7 nm. This can be associated with shell (~3.5 nm) around the particles which is apparent in I_c function, but not in scattering on H_2O-based sample. In MA sample the $p(r)$ functions coincide, so in this sample the aggregates consist of nanomagnetite with one incomplete layer of the surfactant [21,22].

In case of maghemite water-based ferrofluid stabilized by short citric ions (charge stabilization [25]) the particles can be considered as homogeneous [26]. The Coulomb interaction is compensated with the addition of NaCl to the solvent. In that case, the result of SANS contrast variation experiment gives directly two characteristic sizes of the particles – nuclear and magnetic [18]. The dependence of the gyration radius on contrast together with its fit is presented in Fig. 10.

The difference in magnetic and nuclear radii of around 3 nm could hardly be explained as the existence of magnetically dead layer on the edge of maghemite nanoparticles in the ferrofluid. As it was shown such a difference can be explained as a result of non-uniform charge distribution on the surface of the particles and as a result the existence of residual Van der Waals interaction (for more details refer to [26]).

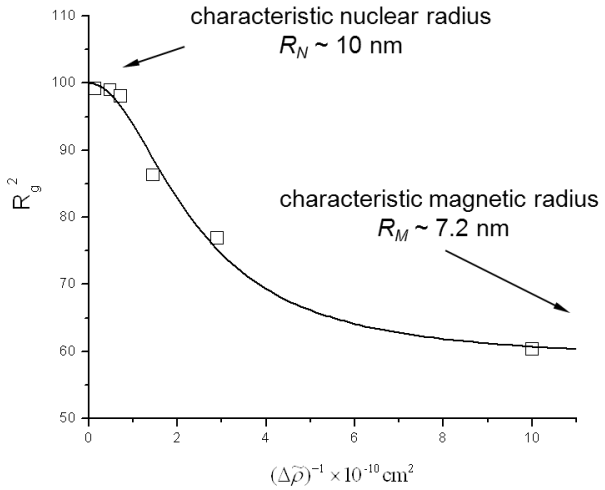

Fig. 10: *The dependence of the gyration radius on contrast and its fit according to [18].*

4.3 Polarized neutrons. Magnetic scattering

When polarised neutrons are used with the neutron spins aligned antiparallel (+) or parallel (−) to the direction of an applied magnetic field H scattering intensity depends on the neutron spin state [27,28,19]:

$$I^{+}(q) = F_N^2(q) + [F_M^2(q) - 2F_N(q)F_M(q)]\sin^2\varphi, \qquad (14a)$$

$$I^{-}(q) = F_N^2(q) + [F_M^2(q) + 2F_N(q)F_M(q)]\sin^2\varphi, \qquad (14b)$$

where φ is azimuthal angle in detector plane.

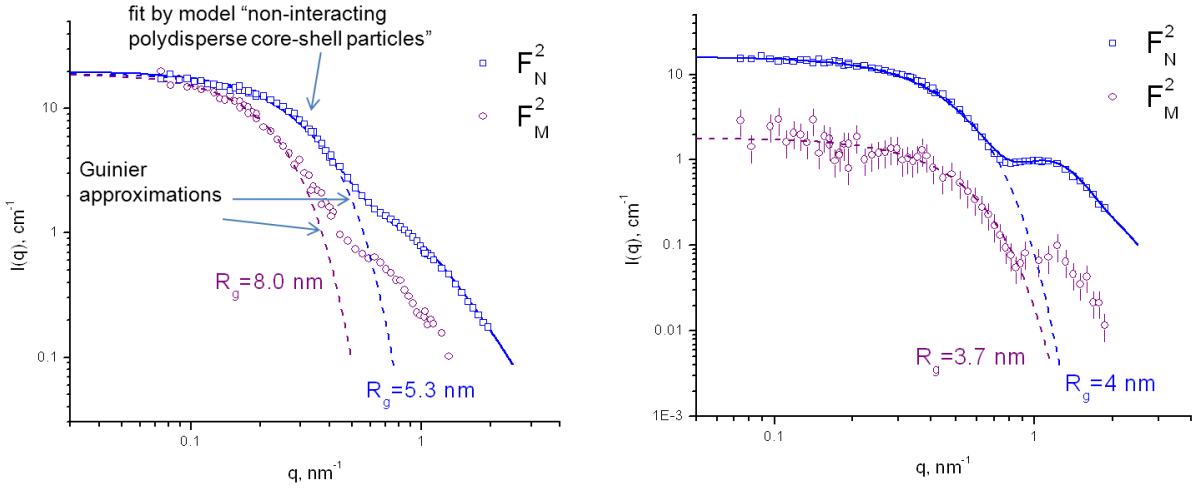

(a) (*b*)

Fig. 11: *Separation of nuclear and magnetic scattering contributions for magnetite ferrofluids based of deuterated cyclohexane and stabilized with oleic (a) and myristic acid (b).*

Thus, character of the scattering is anisotropic now. By making cuts of scattering pattern for both intensities in sectors 0° with 180° and 90° with 270° and solving the system of equations (14) one can separate nuclear F_N and magnetic F_M contributions [29,30]. Separation of nuclear and magnetic scattering on the example of organic ferrofluid is represented in Fig. 11. Different magnetic and nuclear radii calculated from Guinier approximation point to a complex correlation between the magnetic moments of the particles. These correlations differ qualitatively for the two samples [30].

When a polarization analysis of the scattered beam is applied four types of scattering processes are distinguished, two for conserving the neutron spin $(F^{++})^2$ and $(F^{--})^2$ (non spin flip scattering, NSF) and two with reversal of the spin with the scattering $(F^{+-})^2$ and $(F^{-+})^2$ (spin-flip scattering, SF) [27,28,19]. In a particle of radius 4 nm, about 50 % of atoms lie on the surface. The concept of a well-defined super-moment breaks down. Single domain nanoparticles still have uniform magnetization direction, but their spin configuration is not so transparent [31]. In real particles, the surface region thickness is very sensitive to particle shape distortion, surface roughness, surface impurities, defects (like vacancies), compositional inhomogeneity, surface chemical bonds with environment, etc [12]. In literature one can find several possible descriptions of particle spin configuration (see for example [32]).

For the first time the magnetically distinctive core-shell morphology was “seen” in the work [33], where the polarization analysis was successfully applied to directly extract the average spatial distributions of magnetic moments and their correlations. From the obtained scattering in perpendicular direction to the applied magnetic field the authors conclude that magnetic shells of nearly uniform magnitude and direction around the magnetic core exist.

5 Conclusions

Magnetic nanoparticles in general and magnetic fluids particularly nowadays are widely used in technics and are very promising for biomedical applications. For the latter case structure and properties of the substances have to be known beforehand in order to control the synthesis process. The small-angle neutron scattering together with contrast variation technique plays a crucial role in particle structure definition. The newly developed approach of basic functions in contrast variation experiments for the case of polydisperse magnetic nanoparticles opens new possibilities for structural determination. Compared to the monodisperse case, the contrast dependence of scattering integral parameters for the polydisperse system contains a number of additional parameters comprising information about polydispersity function of the system; their analysis increases the reliability of experimental results. As to the SANS data fitting according to supposed particle models the contrast variation technique results in additional parameters, which can be included in the fit function as constants, thus reducing the number of free parameters and increasing the reliability of the fit.

Acknowledgements: the author would like to thank colleagues without whom this work would have not been possible: M.V. Avdeev, V.L. Aksenov (FLNP JINR, Russia), L.A. Bulavin, V.I. Petrenko (Physics Department KNU, Ukraine), L. Vekas, D. Bica [1952-2008], O. Marinica (Laboratory of Magnetic Fluids CFATR, Romania), V.M. Garamus, R. Willumeit (HZG, Germany), E. Dubois, R. Perzynski (UPMC, France).

References

[1] R.E. Rosensweig, Ferrohydrodynamics, Cambridge University Press 1985.
[2] D. Bica, L. Vekas, M.V. Avdeev, et al.: *J Mag Mag Mater* 311 (2007) 17-21.
[3] M.V. Avdeev, V.L. Aksenov, M. Balasoiu, et al., *J Coll Interface Sci* 295 (2006) 100-107.
[4] S. Odenbach (Ed.), Colloidal Magnetic Fluids: Basics, Development and Application of Ferrofluids, *Lect. Notes Phys.* 763, Springer, Berlin Heidelberg 2009.
[5] C. Scherer, A.M. Figueiredo Neto, *Braz J Phys*, 35(3A) (2005) 718-727.
[6] N.A. Brusnetsov, T.N. Brusnetsova, E.Yu.Filinova, et al., *J Mag Mag Mater* 311 (2007) 176-180.
[7] C. Sun, J.S.H. Lee, M. Zhang, *Advanced Drug Delivery Reviews* 60(11) (2008) 1252-1265.
[8] Q.A. Pankhurst, J. Connolly, S.K. Jones and J. Dobson, *J Phys D Appl Phys* 36 (2003) R167-181.
[9] N.A. Brusentsov, L.V. Nikitin, T.N. Brusentsova, et al., *J Mag Mag Mater* 252 (2002) 378-380.
[10] T.N. Brusentsova, V.D. Kuznetsov, *J Mag Mag Mater* 311 (2007) 22-25.
[11] D. Sellmyer, R. Skomski (Eds.), Advanced Magnetic Nanostructures, Springer 2006.
[12] S.P. Gubin (Ed.), Magnetic Nanoparticle, WILEY-VCH Verlag GmbH & Co. KGaA, Weinheim 2009.
[13] C.A. Ross, *Annu Rev Mater Res* 31 (2001) 203-235.
[14] J.L. Dormann, D. Fiorani, E. Tronc, Magnetic Relaxation in Fine-Particle Systems, in I. Prigogine, S.A. Rice (Eds.), *Adv Chem Phys* 98, John Wiley & Sons, Inc., Hoboken, NJ, USA 2007.
[15] G. Porod, General Theory, in O. Glatter, O. Kratky (Eds.), Small Angle X-ray Scattering, Academic Press Inc. (London) Ltd., 1982.
[16] L.A. Feiging, D.I. Svergun, Structure Analysis by Small-Angle X-Ray and Neutron Scattering, Plenum Press, New York 1987.
[17] H.B. Stuhrmann, Contrast Variation, in O. Glatter, O. Kratky (Eds.), Small Angle X-ray Scattering, Academic Press Inc. (London) Ltd., 1982.
[18] M.V. Avdeev, *J Appl Cryst* 40 (2007) 56-70.
[19] A. Wiedenmann, *Physica B* 356 (2005) 246-253.
[20] A.V. Feoktystov, M.V. Avdeev, V.L. Aksenov, et al., *Solid State Phenom* 152-153 (2009) 186-189.
[21] A.V. Feoktystov, L.A. Bulavin, M.V. Avdeev, et al., *Ukr J Phys* 54 (2009) 266-273.
[22] M.V. Avdeev, B. Mucha, K. Lamszus, et al., *Langmuir* 26(11) (2010) 8503-8509.
[23] M.V. Avdeev, V.L. Aksenov, M. Balasoiu, et al., *J Coll Interface Sci* 295 (2006) 100-107.
[24] J. Skov Pedersen, *Adv Coll Interface Sci* 70 (1997) 171-210.
[25] R. Massart, E. Dubois, V. Cabuil and E. Hasmonay, *J Magn Magn Mater* 149 (1995) 1-5.
[26] M.V. Avdeev, E. Dubois, G. Mériguet, et al., *J Appl Cryst* 42 (2009) 1009-1019.
[27] R.M. Moon, T. Riste, W.C. Koehler, *Phys Rev* 181(2) (1969) 920-931.
[28] R. Pynn, J.B. Hayter, S.W. Charles, *Phys Rev Lett* 51 (1983) 710-713.

[29] M.V. Avdeev, M. Balasoiu, V.L. Aksenov, et al., *J Magn Magn Mater* 270 (2004) 371-379.
[30] M. Balasoiu, M.V. Avdeev, A.I. Kuklin, et al., *Rom Rep Phys* 58(3) (2006) 305-311.
[31] R.A. Kodama, A.E. Berkowitz, *Phys Rev B* 59 (1999) 6321-6336.
[32] Y. Labaye, O. Crisan, L. Berger, et al., *J Appl Phys* 91 (2002) 8715-8717.
[33] K.L. Krycka, R.A. Booth, C.R. Hogg, et al., *Phys Rev Lett* 104 (2010) 207203.